Advancing Label-Free Biosensing Technologies Using Integrated Optical Circuits

R. Favaretto[1,2,3][0009-0006-8200-9958], N. Ardoino[2][0009-0007-4837-254X], G. Pucker[3][0000-0002-9338-8686], M. Bernard[3][0000-0002-0374-3681], N. Bellotto[2][0000-0002-7701-9186], N. Srocka[2] and C. Guardiani[2][0009-0007-6134-4332]

[1] Department of Physics, University of Trento, via Sommarive 14, 38123, Trento
[2] FTH S.r.l., via Sommarive 18, 38123, Trento
[3] Fondazione Bruno Kessler, via Sommarive 18, 38123, Trento
rachele.favaretto@unitn.it

Abstract. Biosensors are powerful tools for detecting specific molecules by leveraging biological interactions to generate measurable signals. This research focuses on the development of advanced label-free biosensors using Silicon Nitride integrated optical circuits, employing Mach-Zehnder Interferometer (MZI) structures as the sensing elements. MZIs, which combine waveguiding and interferometry, offer high sensitivity by detecting phase shifts induced by analyte binding in real time. The development process encompasses component simulation, chip design, chip fabrication, packaging, optical and electrical characterization and biological testing. Although the Silicon Nitride sensor is still under development, preliminary results from silicon waveguide-based MZI devices have demonstrated their ability to accurately monitor binding kinetics. A key advantage of Silicon Nitride is its compatibility with visible wavelengths, where optical losses are lower when using aqueous cladding, as is common in biological testing. This research holds significant potential for advancing label-free optical biosensing technologies, with applications spanning healthcare, environmental monitoring, and beyond.

Keywords: Biosensor, Mach-Zehnder Interferometer, Photonic Integrated Circuit, Silicon Nitride, Label-free Detection, Point of Care.

Biosensors are innovative tools that leverage the specificity of biological interactions to detect molecules of interest, such as proteins, viruses or bacteria. The analyte binds to a bio-recognition element (like an antibody or aptamer), triggering a reaction that is converted into a measurable signal by a transducer. The sensitivity of the sensor is defined as the output response per unit change of the total quantity of the target analyte molecules bound to the surface of the waveguide.

Waveguide-based optical biosensors are particularly interesting because they can be used as label-free sensors directly binding the biorecognition elements on their surface and because they can be integrated into miniaturized lab-on-chip technologies.

The light is directed in the waveguide, a transparent material with a refractive index higher than its surrounding environment, the silicon oxide substrate and the biofluid. What is important for sensing is the fact that the electric field is not strictly confined in the waveguide but has exponentially decaying tails in the surrounding materials as shown in Fig. 1. Any refractive index changes near to the waveguide surface, like the one caused by the specific binding of an analyte to an antibody, yields to a detectable change of the effective refractive index of the mode.

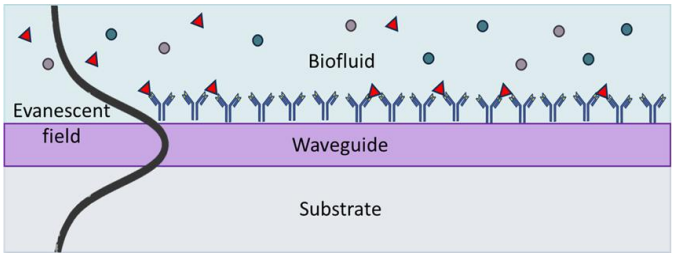

Fig. 1 Schematic of a biofunctionalized slab waveguide**.**

Among the various types of waveguide-based optical biosensors, microring resonators and integrated asymmetric Mach–Zehnder interferometers (MZIs) are among the most extensively studied. In particular, waveguide interferometers hold significant importance due to their ability to combine two highly sensitive techniques—optical waveguiding and interferometry—resulting in biosensors with enhanced sensitivity, well-suited for point-of-care applications [1]. The sensing mechanism [2] can be schematically described as follows. The input light beam is directed to the sensor's input and then equally split into two arms. One arm, the sensing arm, is biofunctionalized with biorecognition elements on the surface for detection, while the other, the reference arm, includes a phase shifter. The light is then recombined using a 2x2 coupler. The output optical power is converted by a photodiode into two complementary current signals having the shape of squared sine and cosine waves modulated by the phase difference between the two arms. When a binding event occurs, the refractive index of the medium around the sensing arm changes, introducing a phase shift. This phase shift can be counterbalanced by the phase shifter in the control arm.

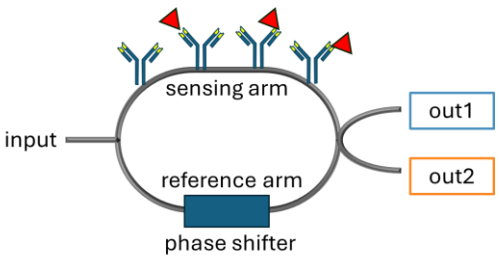

Fig. 2 Schematic of a Mach-Zehnder Interferometer bio sensor**.**

The power used to maintain the MZI in phase is proportional to the amount of analyte bound in the sensing arm, providing a quantitative measurement of the analyte concentration in the biofluid. A sketch of a MZI biosensor is shown Fig. 2.

The workflow to develop a biosensor based on Mach-Zehnder interferometers includes several key steps. In the first step, the key optical components are thoroughly simulated; then the integrated optical circuit is designed; the third step entails fabricating the circuit; and finally, the resulting physical structure is fully characterized by means of optical and biological tests.

Optical Component Simulation

The design of an optoelectronic biosensor chip begins with the selection of an appropriate operating wavelength. Photonic biosensors typically operate within the visible spectrum, as water, the primary constituent of most biofluids, exhibits minimum optical absorption in this range. Nonetheless, in a previous project, we employed the 1550 nm telecom wavelength using a silicon waveguide platform. Despite the relatively high absorption losses in water (~10 dB/cm), this wavelength offers practical advantages: it is supported by multiple foundries and chip fabrication at this wavelength is both mature and cost-effective, yielding reproducible results. In the present work, we investigated both the telecom-band (1550nm) and near-visible band (780nm), to evaluate their respective advantages in terms of technical performance and industrial scalability.

1 Waveguide geometry

Following the selection of the operating wavelengths, the next step involved the simulations of key photonic chip components. A fundamental design decision at this stage was the determination of the optimal waveguide geometry, as this constitutes the fundamental building block of all optical components on the chip.

Simulations were conducted for waveguides with heights of 150 nm and 350 nm and widths ranging from 500 nm—the lithographic current resolution limit achievable at FBK cleanroom—to 2500 nm. A schematic of the simulated cross-section is shown in Fig. 3a while Fig. 3b illustrates a representative example of the resulting electric field. The simulations were performed using *modesolverpy* Python library. The structure consists of a silicon substrate with a 5 µm bottom oxide layer, overlaid by a silicon nitride waveguide with parameterized height and width. Finally, the cladding was evaluated in two configurations: water and oxide.

a

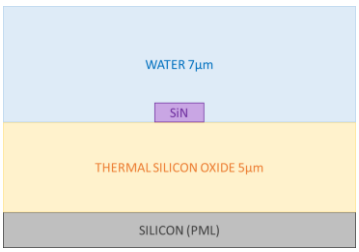

b

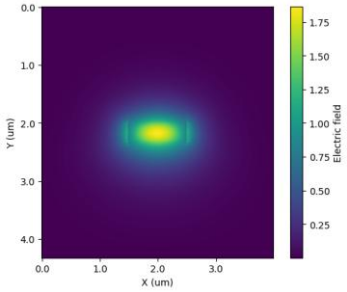

Fig. 3a Cross-sectional design of the simulation window, from bottom to top: Silicon substrate, bottom oxide layer, Silicon nitride waveguide, water cladding. **3b** Example of the simulated electric field in the waveguide. The boundary conditions for the simulation are PML**.**

The simulation allowed us to calculate both the real and imaginary parts of the effective refractive index of the guided mode(s) as well as the spatial distribution of the electric field at each point within the simulation window. Key parameters that could be extracted from the simulation included the effective refractive index of guided modes, mode confinement within the waveguide core, mode fraction, absorption losses and bulk sensitivity — a metric that quantifies the sensitivity of the effective refractive index to variations in the cladding refractive index.

Only parameter combinations with water cladding that supported single-mode waveguides (TE00) and acceptable optical losses— defined as absorption below -15 dB/cm—were considered for further analysis. The 780 nm wavelength with a waveguide height of 350 nm was excluded, as it did not support single mode within the tested width range. Configurations wl780nm-h150nm and wl1550nm-h350nm exhibited slightly higher effective indices than wl1550nm-h150nm, resulting in less confined optical modes. All configurations demonstrated a high TE mode fraction. As expected, wl1550nm designs showed increased absorption losses in water but offered somewhat better sensitivity. The results for refractive index, optical absorption losses, and bulk sensitivity are reported in Fig. 4.

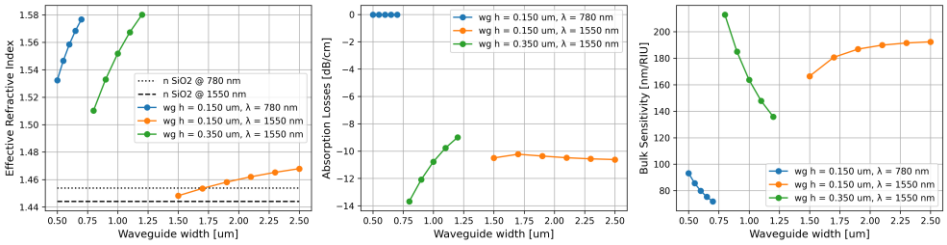

Fig. 4 Results of the simulations (water cladding) for the effective refractive index, absorption losses and bulk sensitivity of the 3 configurations wl780nm-h150nm, wl1550nm-h150nm and wl1550nm-h350nm in the widths range allowing single-mode TE00 propagation**.**

Among the valid configurations, a trade-off analysis considering loss, sensitivity, and the lithographic constraints of FBK fabrication process led to the selection of wl780nm-h150nm-w600nm, wl1550nm-h150nm-w2100nm and wl1550nm-h350nm-w1000nm.

1.1 Bending radius

Following the selection of the waveguide cross-sections, additional simulations were conducted to determine their minimum bending radii required to maintain low optical losses due to curvature. This was assessed by comparing the effective indices of bent vs. straight waveguides, within a <0.003% tolerance for the difference. The

results indicated that the wl1550nm-h150nm-w2100nm waveguide required a minimum bending radius of approximately 600 µm— due to weak mode confinement — which was unsuitable for compact chip layouts. In contrast, the 780 nm and 1550 nm configurations exhibited significantly smaller bending radii (~80 µm and ~150 µm respectively) and were thus retained for further development.

2 Simulation of the Directional couplers

Following definition of the two operating wavelengths and of their respective minimum bending radii, the next design step was to simulate the couplers required for the MZI configuration. One common method for implementing waveguide couplers is by using straight parallel sections where the evanescent field of one overlap with that of the adjacent guide, forming a directional coupler. This configuration allows optical power to transfer gradually from one waveguide to the other. By carefully optimizing the gap between the guides and the length of the coupling region, the coupling ratio can be precisely controlled. For our case the target splitting ratio was 50:50.

The first step to calculate the optimal coupling length L is to determine the refractive indices of the two modes propagating in the coupled waveguide system. The difference between these indices, Δn, is calculated. Assuming that initially all the input power is in waveguide 1 the coupling length to achieve a desired power transfer to waveguide 2, can be determined by solving Eq. (1):

$$L = [\lambda/(\pi \cdot \Delta n)] \cdot \sin^{-1}[(P_2/P_1)^{1/2}] \quad (1)$$

The following table provides a summary of the resulting values that were found in this case.

Table 1. Table captions should be placed above the tables.

Wavelength	Height	Width	Coupler gap	Coupler width
780 nm	150 nm	600 nm	600 nm	103.5 um
1550 nm	350 nm	1000 nm	835 nm	50 um

Chip design

The sensor integrates all components onto a single photonic chip, including the optical input/output interfaces, waveguides, MZIs arms exposed to analyte-containing fluids, and metal structures for phase shifting.

As illustrated in Fig. 5 the chip layout is organized as follows: the left side hosts one optical input and 16 optical outputs. The middle section accommodates the phase shifters while all the MZI sensor are placed on the right side of the chip. This floorplan has been chosen to allow for a sharp separation between optical and electro-optical components –namely the phase shifters.

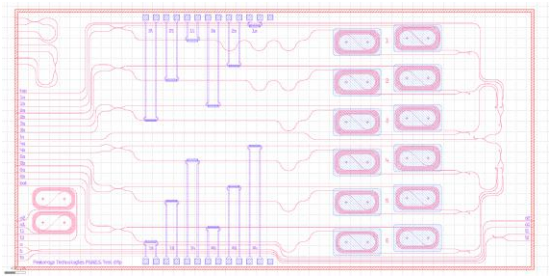

Fig. 5 Layout of the chip for telecom wavelength.

A well is etched above each MZI to allow biofluids to interact with the sensing region. This is accomplished by selectively removing the oxide dielectric above the interferometer arms through a combination of dry and wet etching processes. The exposed length of each MZI arm is varied across different instances in order to study the impact of interaction length on the sensor's sensitivity. In addition to MZI arm length, a second key parameter that is varied is the optical path difference (ΔL) between the two arms. This variation is intended to evaluate the optimal tradeoff between free spectral range (FSR) and sensitivity.

Chip fabrication and packaging

The design is realized through precise photolithographic processes, using multiple masks to pattern waveguides, metal structures, pad opening, sensor window areas and finally deep trenches and facets. Previous fabrication experience [3] has informed the current chip designs to ensure robustness and manufacturability. The next steps are packaging via wire bonding to a custom-designed PCB and encapsulation with the microfluidic chamber. The chip will then be used with the Diamir2 diagnostic readout machine, owned by FTH S.r.l.

Biological testing

After fabrication, the biosensor's functionality is validated using biological tests. Although the Silicon Nitride MZI-based sensor is still under fabrication, preliminary results from Silicon MZI sensors provide a basis for characterizing analyte-antibodies interactions, monitoring binding kinetics.

The Fig. 6 below shows an example of an outcome of a biological test on a Silicon MZI sensor, using a sandwich strategy to enhance the signal output. MZIs 2 and 6 were functionalized with a-CRP antibodies, MZIs 4 and 5 with a-PCT antibodies, and MZI 3 served as a reference. The sensors are primed with a buffer solution, then the bio-fluid with 0.1 nM CRP and 1 nM PCT protein is flowed on top of the sensors to bind the analytes. Finally, a step with two detection antibodies is applied after a short

buffer cleaning step to complete the test sequence. The binding behavior matches theoretical models [3] and is consistent with previous experimental results in the literature, such as [4], which employs a similar integrated MZI setup, though without a phase shifter, thus confirming the feasibility of MZI-based optical sensors for real-time quantitative analysis.

Fig. 6 Example of biological test.

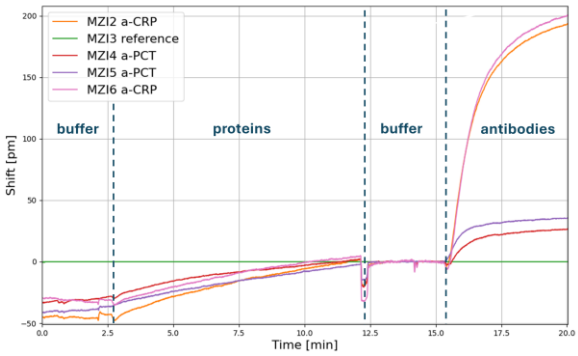

While the fabrication of Silicon Nitride MZI-based biosensors is ongoing, this research holds significant promise for advancing label-free optical biosensing technologies. Key goals include achieving enhanced sensitivity, reducing optical losses and signal-to-noise ratios, and integrating alternative phase-shifting mechanisms to improve sensor performance.

Acknowledgments

This research was supported in part by the Autonomous Province of Trento, L.P. 6 luglio 2023, n. 6 e ss.mm.ii., project FANES Cup: C69J24000350001.

References

1. A. Armani, T. Chalyan, D. Sampson (Eds.). Biophotonics and Biosensing: From Fundamental Research to Clinical Trials Through Advances of Signal and Image Processing. 1st Edition, pp. 15-41. Elsevier (2024).
2. Patent “Dispositivo opto-elettronico per la rilevazione di una sostanza dispersa in un fluido” Filed 23-01-2017 N. 102017000006640 Issued: 27/09/2019
3. R. Favaretto, N. Ardoino, G. Pucker, N. Bellotto, M. Mancinelli, G. Piccoli, M. Bernard, L. Vanzetti, C. Potrich, L. Lunelli, C. Pederzolli, C. Guardiani, L. Pasquardini. A ring resonators optical sensor for multiple biomarkers detection. Talanta, 282 (2025).
4. Besselink, G.; Schütz-Trilling, A.; Veerbeek, J.; Verbruggen, M.; van der Meer, A.; Schonenberg, R.; Dam, H.; Evers, K.; Lindhout, E.; Garritsen, A.; et al. Asymmetric Mach–Zehnder Interferometric Biosensing for Quantitative and Sensitive Multiplex Detection of Anti-SARS-CoV-2 Antibodies in Human Plasma. Biosensors, 12, 553 (2022).